Magnetic Resonance in Medicine 63:537–542 (2010)

Design and Use of Variable Flip Angle Schedules in Transient Balanced SSFP Subtractive Imaging

Travis Smith,[1]* Zungho Zun,[1] Eric C. Wong,[2] and Krishna S. Nayak[1]

In subtractive imaging modalities, the differential longitudinal magnetization decays with time, necessitating signal-efficient scanning methods. Balanced steady-state free precession pulse sequences offer greater signal strength than conventional spoiled gradient echo sequences, even during the transient approach to steady state. Although traditional balanced steady-state free precession requires that each excitation pulse use the same flip angle, operating in the transient regimen permits the application of variable flip angle schedules that can be tailored to optimize certain signal characteristics. A computationally efficient technique is presented to generate variable flip angle schedules efficiently for any optimization metric. The validity of the technique is shown using two phantoms, and its potential is demonstrated in vivo with a variable angle schedule to increase the signal-to-noise ratio (SNR) in myocardial tissue. Using variable flip angles, the mean SNR improvement in subtractive imaging of myocardial tissue was 18.2% compared to conventional, constant flip angle, balanced steady-state free precession ($P = 0.0078$). Magn Reson Med 63:537–542, 2010. © 2010 Wiley-Liss, Inc.

Key words: variable flip angle; transient; balanced; SSFP; subtractive imaging

Tissue characterization by MRI often involves the subtraction of images obtained with two different preparations of the longitudinal magnetization that encode the specific behavior of interest in the difference signal. Methods such as arterial spin labeling (1), subtraction angiography (2,3), displacement encoding with stimulated echoes (DENSE) (4), and new approaches to T_2 mapping (5) follow this paradigm. The detected difference signal is proportional to the differentially prepared longitudinal magnetization, which decays to zero due to T_1 relaxation. Since the magnitude of the difference signal diminishes with time, these subtractive imaging studies can be hampered by low signal-to-noise ratio (SNR) (6).

The use of efficient segmented sequences such as balanced steady-state free precession (bSSFP) to capture this diminishing difference signal is gaining acceptance (2,5–9). As opposed to single-shot imaging using spiral or echo planar trajectories, snapshot bSSFP sequences have reduced sensitivity to off-resonance and the potential for improved spatial resolution and coverage (10). Steady-state behavior appears because each pulse repetition time (TR) interval has the same gradient area and radiofrequency flip angle. Prior to this, the magnetization is in a transient state, characterized by an oscillatory progression toward the steady state (11). In a subtractive imaging scenario, data must be acquired in the transient state because the differential magnetization is zero in the steady state. Stabilization techniques have been developed to minimize early oscillations and make the transient state useful for data collection (11,12).

In this work, we remove the constraint that every excitation must have the same flip angle. Varying the flip angles during data acquisition allows us to design flip angle schedules to enhance or suppress certain characteristics of the difference signal. For example, to maximize SNR we may construct a variable flip angle (VFA) schedule to optimize the detected signal difference between the differentially prepared scans. Because both scans use the same TR, receiver bandwidth, and resolution, their noise statistics would be identical and any signal increase would come from the application of the VFA schedule. Such schedules may be designed to optimize any function of the difference signal.

This work presents an efficient technique to generate VFA schedules optimized for the detection of difference signals in transient bSSFP acquisitions. The validity of the proposed method is examined using phantoms and compared with conventional, constant flip angle (CFA) acquisitions in vivo.

MATERIALS AND METHODS

Flip Angle Schedule Generation

The generation of VFA schedules consisted of two steps: characterization of the object or tissue of interest, followed by numerical optimization of an objective function of the tissue's simulated difference signal. In the characterization step, intrinsic properties of the tissue were measured for later use in the simulation. These include the T_1 and T_2 relaxation times and the in-slice distributions of resonant offsets and amplitude of radiofrequency field (B_1) scale factors. A distribution of flip angles was also calculated from the slice profile of the radiofrequency excitation pulse and convolved with the B_1 scale distribution. Relative histograms of the off-resonance spectrum and flip angle scale factors were created from these distributions.

These measurements were used in a Bloch equation simulator to estimate the difference signal acquired from the tissue using a VFA bSSFP sequence. The simulator tracked a large number of differential magnetization vectors in the rotating frame as they nutated from radiofrequency excitations and precessed due to off-resonance. One three-dimensional vector was tracked for each isochromat and each scale factor, and a weighted average of

[1]Ming Hsieh Department of Electrical Engineering, University of Southern California, Los Angeles, California, USA

[2]Departments of Radiology and Psychiatry, University of California, San Diego, La Jolla, California, USA

*Correspondence to: Travis Smith, M.S., 3740 McClintock Ave, EEB 412, University of Southern California, Los Angeles, CA 90089-2564.
E-mail: traviss@usc.edu

Received 21 February 2009; revised 13 September 2009; accepted 24 September 2009.

DOI 10.1002/mrm.22255
Published online in Wiley InterScience (www.interscience.wiley.com).

all magnetization vectors was calculated once per TR (at the echo time) using the weights from the relative histograms. We simulated 251 isochromats linearly spaced across the 1/TR steady-state free precession bandwidth and 15 scale factors linearly spaced across the measured range of flip angle scale factors (3765 total magnetization vectors). To form the final simulated difference signal, the transverse components of the resulting vectors were stored in a complex array of length N, where N is the number of TRs in the data acquisition interval. Inputs to the simulator were the array of flip angles; the TR, T_1, and T_2 times; arrays of isochromats and their relative histogram; and arrays of scale factors and their relative histogram.

In the optimization step, an objective function of the difference signal was supplied to a multistage optimization algorithm. The Bloch equation simulation ran numerous times as the objective function was evaluated for various flip angle schedules during the course of the optimization. The result was the optimal N-angle schedule, which consisted of a linearly increasing sequence of flip angles to help stabilize early transient oscillations, followed by the N flip angles in the data acquisition interval. Including the stabilization duration as a parameter allowed the optimization to balance the tradeoff between signal stabilization and signal decay.

Rather than perform a single, high-dimensional optimization, which would be sensitive to the initial guess and prohibitively time consuming for even moderate values of N, our multistage algorithm efficiently approached the optimal result by using a sequence of optimizations with progressively larger dimensionalities yet progressively more informed initial guesses. The N-angle schedule was represented by a piecewise constant function that was parameterized by the number of pieces, or segments, F (see Appendix). With this parameterization, a complete N-angle schedule could be represented with F numbers ($1 \leq F \leq N$). In any particular stage, only F values were optimized, along with the duration of the stabilization period, making the dimensionality of that stage's optimization $F + 1$. In the first stage, $F = 1$ and the optimal constant angle schedule was found. The second stage used $F = 4$, and as the stages progressed, F increased by 2 until the last stage (the N/2th stage) in which $F = N$ and the algorithm terminated. Each stage produced a full N-angle schedule that became the initial guess for the following stage. The N-angle schedule generated in the last stage was the final VFA schedule.

In the first stage, a two-dimensional exhaustive search was used to find the globally optimal constant angle schedule. All subsequent stages used a sequential quadratic programming routine to perform the optimizations. Sequential quadratic programming is a class of iterative, nonlinear, constrained optimization methods similar to the Newton-Raphson algorithm, except that the constraints are incorporated using Lagrange functions (13). Each sequential quadratic programming iteration solves a quadratic program subproblem consisting of a local quadratic approximation of the objective function and a local linear approximation of the constraints. We used the sequential quadratic programming routine in MATLAB (Mathworks, Inc, South Natick, MA), which employs an active set strategy to solve each quadratic program subproblem (14).

We considered three simple objective functions, listed below. Here, $\Delta M_{xy}[k]$ is the value of the complex transverse difference signal at the echo time of the kth TR interval, and $\mu|\Delta\text{Mxy}|$ and $\sigma|\Delta\text{Mxy}|$ are the mean and standard deviation of the detected difference signal, respectively. Each function was minimized in the optimization. Equation 1 is the objective function to maximize the SNR for a delta function impulse response. Equation 2 maximizes the minimum detected difference signal, and Eq. 3 attempts to minimize the apodization along the phase-encode direction without driving the signal toward low SNR.

$$-\left|\sum_{k=1}^{N}\Delta M_{xy}[k]\right| \quad [1]$$

$$-\min_{k}\left\{\left|\Delta M_{xy}[k]\right|\right\} \quad [2]$$

$$\sigma_{|\Delta M_{xy}|}/\mu_{|\Delta M_{xy}|} \quad [3]$$

In our experiments, VFA schedules were generated for TR = 3.2 ms and $N = 96$. The maximum stabilization duration was constrained to 10 pulses, and the maximum prescribed flip angle was limited to 70°, based on a time-bandwidth product of 2.0, maximum pulse duration of 480 μsec, and peak B_1^+ of 0.16 G.

Phantom Experiment

To test the VFA schedules, we constructed a simple spin-warp pulse sequence consisting of two snapshot bSSFP acquisition intervals separated by a nonselective B_1- and amplitude of static field–insensitive saturation pulse (15) to act as the preparation. Both acquisition intervals used the same scanning parameters and the same flip angle schedule to modulate the amplitudes of the slice-selective excitation pulses.

Two phantoms, a cylindrical deionized water phantom (#1) and a spherical dimethyl silicone, gadolinium-doped phantom (#2), were used to assess the accuracy of the simulation and test the multistage optimization strategy. The T_1 and T_2 values were determined from spin echo sequences with and without inversion recovery, respectively, for phantom #1 (TR = 7 sec; spin echo-inversion recovery: 10 inversion times ranging from 0.2–2 sec; spin echo: 10 echo times ranging from 0.1–1.5 sec; $T_1 = T_2 = 1300$ ms) and phantom #2 (TR = 2.1 sec; spin echo-inversion recovery: 10 inversion times ranging from 50–200 ms; spin echo: 10 echo times ranging from 10–100 ms; $T_1 = 300$ ms, $T_2 = 30$ ms). Off-resonance distributions were estimated from an amplitude of static field map created from two gradient echo sequences (echo time = 12 and 15 ms, ± 167 Hz frequency range, 128 × 128, field of view = 20 cm, slice = 10mm, receiver bandwidth = 31.5 kHz). B_1 scale factor distributions were estimated from a B_1 map acquired using the double angle method (16), with TRs equal to those used in the T_1 and T_2 measurements (flip angle = 45° and 90°, 128 × 64, field of view = 20 cm, slice = 10 mm, receiver bandwidth = 31.5 kHz).

VFA schedules corresponding to the objective functions in Eqs. 1–3 were generated for each phantom using the multistage optimization process. Using these schedules, difference signals were simulated and measured using the scanner (standard head coil, field of view = 20 cm, slice = 10 mm, TR = 3.2 ms, receiver bandwidth = 125 kHz). Phase encoding was turned off and the samples at echo time were extracted to compare with the simulations. All measurements were performed on a GE 3-T scanner (Signa Excite HD; GE Healthcare, Waukesha, WI).

In Vivo Experiments

To demonstrate the benefit of this technique in vivo, the SNR of myocardial tissue (T_1 = 1100 ms and T_2 = 40 ms at 3 T) (17) was measured using both variable and constant angle schedules. Nominal off-resonance and B_1 scale distributions of the myocardium (and left ventricular blood pool) measured from eight healthy subjects in a previous study (18) were averaged to create the relative histograms needed for the simulator. Using the objective function in Eq. 1, an optimized VFA schedule was generated. The CFA schedule produced by the first stage of the optimization process established the SNR performance baseline.

With these flip angle schedules, bSSFP cardiac images with linear view ordering were acquired in eight healthy volunteers using a mid short-axis view (eight-channel cardiac coil, 96 × 96, field of view = 22 cm, slice = 10mm, TR = 3.2 ms, receiver bandwidth 125 kHz). For each schedule, two snapshot images were acquired from mid diastole during a breath hold and then subtracted. Volunteers were scanned twice with each schedule. Each detected difference image was manually segmented to isolate the left ventricular myocardium. SNR was calculated from the ratio of the mean myocardial pixel value (from both images) to the standard deviation of a manually identified region of noise pixels (from both images). Subjects were screened for contraindications and provided informed consent in accordance with institutional policy.

RESULTS

Phantom Experiment

The three VFA schedules for each phantom are shown in Fig. 1a and b, respectively. The schedules for Eq. 1 were 70° for almost every TR, indicating that the best schedule under our constraints was (almost) a constant angle one. The schedule generation times for Eqs. 1, 2, and 3 on a 2.6-GHz single-core processor were 8, 20, and 40 min, respectively, for phantoms #1 and 31, and 13 and 112 min, respectively, for phantom #2.

Figure 2a and b shows the difference signal measurements and simulations for each schedule. The signals for phantom #1 are larger because of its longer relaxation times (and slower decay of the differential magnetization). The normalized absolute errors between the simulations and measurements are plotted in Fig. 2c and summarized in Table 1. Across all schedules and both phantoms, the absolute error was 0.92% ± 0.82 (mean ± standard deviation). Because the errors are normalized,

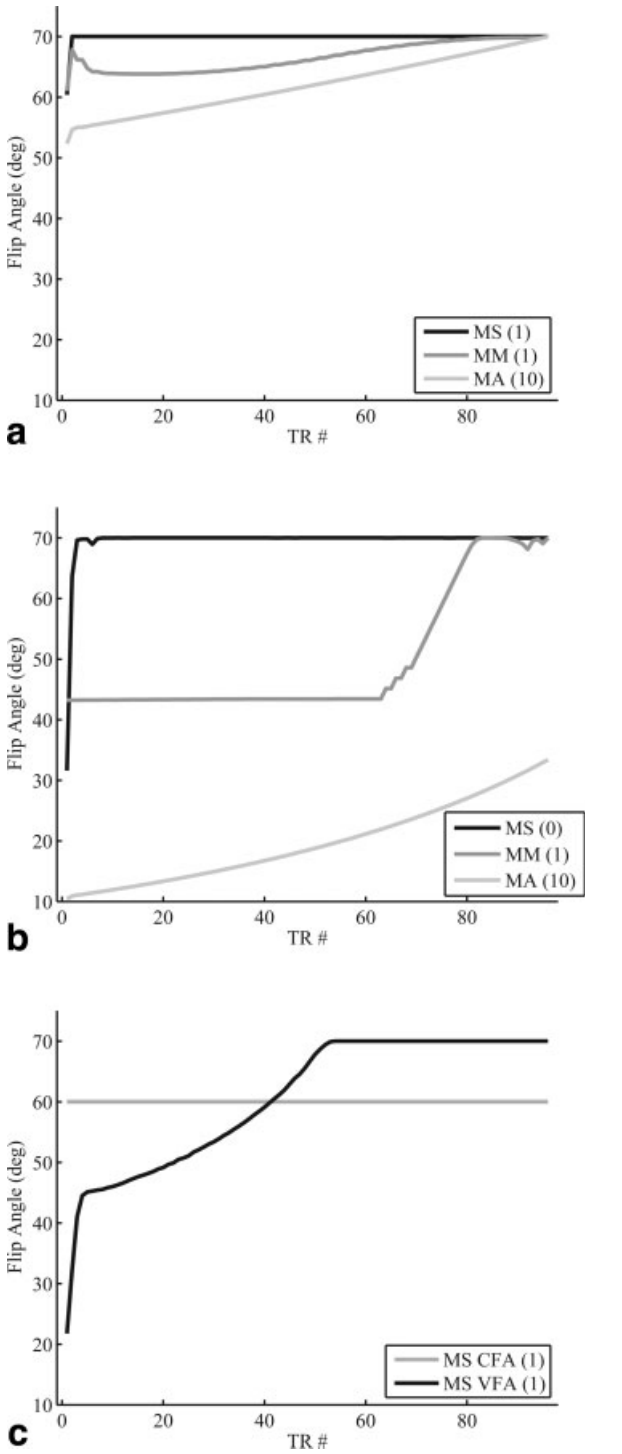

FIG. 1. VFA schedules for a 96-tip data acquisition optimized for (**a**) phantom #1 (T_1/T_2 = 1300/1300 ms), (**b**) phantom #2 (T_1/T_2 = 300/30 ms), and (**c**) myocardial tissue (T_1/T_2 = 1100/40 ms). The baseline CFA schedule is also shown for the myocardium. Flip angle schedules are displayed for three objective functions: the maximum sum (MS) function in Eq. 1, the maximum minimum (MM) function in Eq. 2, and the minimum apodization (MA) function in Eq. 3. The optimized stabilization duration for each schedule appears in parentheses.

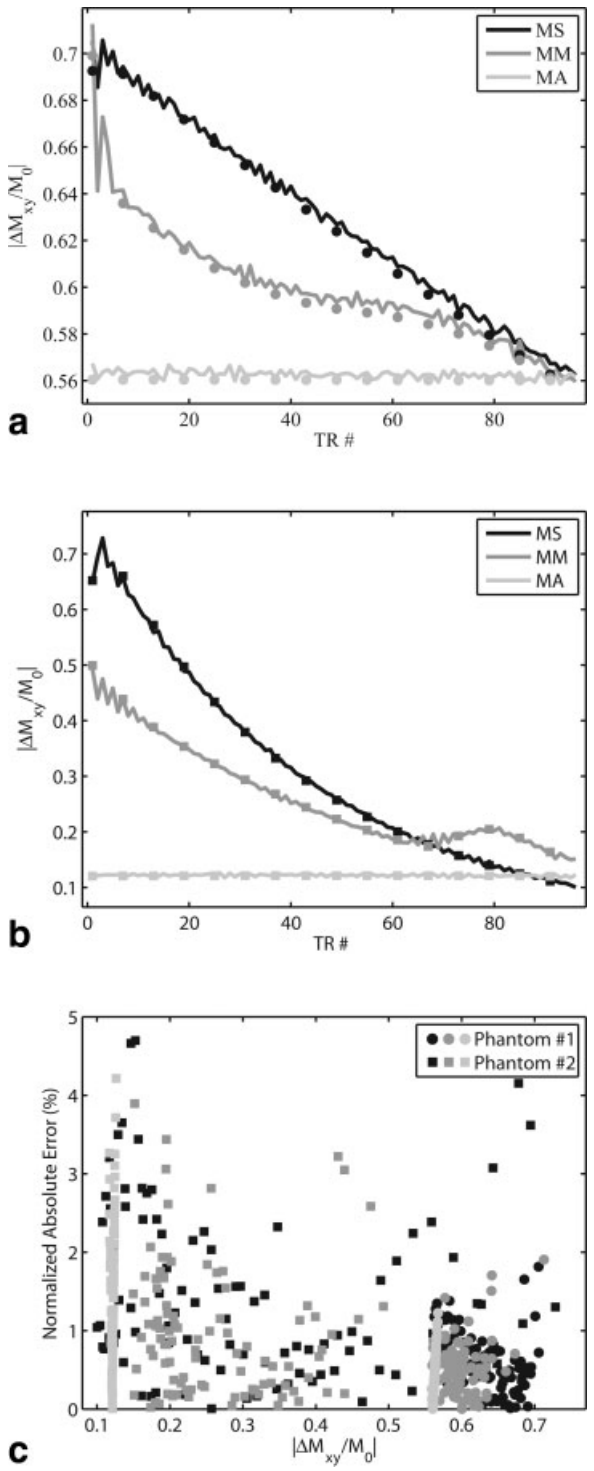

FIG. 2. Phantom results using the optimized VFA schedules indicating close correspondence between measurement (solid lines) and simulation (shown every 6th TR) for (**a**) phantom #1 (circle markers) and (**b**) phantom #2 (square markers). **c**: Normalized absolute errors between simulation and measurement, defined as $100 \times |\Delta M_{xy,sim} - \Delta M_{xy,meas}| / \Delta M_{xy,meas}$, for each schedule. The slower decay toward steady-state in phantom #1 led to increased signal and smaller errors. Table 1 lists the error statistics for each objective function.

the smaller signals measured in phantom #2 contributed to the larger errors observed therein.

In Vivo Experiments

The flip angle schedules optimized for Eq. 1 and myocardial tissue are displayed in Fig. 1c. The generation time was 42 min for the VFA schedule. The simulated difference signal for each schedule is shown in Fig. 3a. The VFA simulation is larger near the center of *k*-space (at the 49th TR interval), which leads to a higher myocardial signal in the image domain. The SNR measurements from each volunteer are shown in Fig. 3b, and example difference images are shown in Fig. 3c and d.

Compared with the baseline schedule, the VFA schedule produced higher myocardial SNR in every volunteer. The SNR improvement was 18.2% ± 1.4 (mean ± standard deviation). No image artifacts were observed in any VFA image, due in part to the relatively smooth behavior of both the VFA schedule (Fig. 1c) and the expected signal profile (Fig. 3a).

Differences in the SNR measurements from the two schedules were assessed using the paired *t* test, which revealed a statistically significant improvement ($P = 7.5 \times 10^{-5}$) at the 5% level. Considering the small sample size, the Wilcoxon signed-rank test (the nonparametric version of the paired *t* test) was performed to compare the two SNR distributions, and it also yielded a significant result ($P = 0.0078$).

DISCUSSION

The strong agreement in the phantom results demonstrates that the simulator is accurately modeling the differential magnetization behavior when exposed to a sequence of varying flip angles. It also validates the technique as a whole since the same simulator that was used to predict the signal profiles was also used to optimize the flip angle schedules.

We observed that using more than 151 isochromats had no numerically significant effect ($<10^{-10}$) on the simulated signal values. Our results used 251 simulated isochromats to reinforce this observation while keeping the computation time small. Similarly, we chose 15 B_1 scales to adequately capture the distribution of scale factors while maintaining fast simulation times.

With $N = 96$, there were 48 optimization stages performed including the final, 97-D one. For most of the objective functions considered here, the total computational time for all 48 stages was less than 45 min. To put this into perspective, we tried directly generating a VFA schedule for myocardium with Eq. 1 using a 97-D optimization initialized with the best constant angle schedule. After 36 h, it had not reached a solution. Our approach reduces the computational complexity by balancing the fidelity of the piecewise approximation with the proximity of the initial guess to the optimal schedule.

Optimization techniques based on sequential quadratic programming may produce schedules that are not globally optimal when the hypersurface of the objective function in the search space has multiple local minima

Table 1
Summary of Simulation Accuracy Results for Phantom Experiments

	Phantom	Objective function	Simulation error[a]		
			Mean ± SD	Median	Max
Phantom #1	$T_1 = 1300$ ms, $T_2 = 1300$ ms	Eq. 1	0.62% ± 0.37	0.58%	1.82%
		Eq. 2	0.53% ± 0.34	0.51%	1.91%
		Eq. 3	0.45% ± 0.25	0.42%	1.22%
Phantom #2	$T_1 = 300$ ms, $T_2 = 30$ ms	Eq. 1	1.42% ± 1.09	1.06%	4.70%
		Eq. 2	0.99% ± 0.85	0.82%	3.89%
		Eq. 3	1.50% ± 0.89	1.47%	4.21%
Overall			0.92% ± 0.82	0.66%	4.70%

[a]Error is the normalized absolute error percentage, defined as 100 times the absolute value of the difference between simulated and measured values normalized by the measured value.

similar in value to the global minimum. Since the precision with which an excitation pulse tips a magnetic moment is far less than the precision of the computational optimization routine, there will be a set of flip angle schedules for any given objective function that all yield similar performance. Further investigation is needed to determine the best strategy in terms of timeliness and optimality.

The generality of our approach makes it easy to adapt to other applications. The objective functions considered here are only examples; the multistage optimization is compatible with any quantitative metric of the simulated difference signal. The technique can be extended to consider multiple tissues simultaneously. For example, the signal from one or more tissues of interest could be maximized while unwanted signals from other, competing tissues are minimized. It is also amenable to objective functions that treat each component of the difference signal separately since the simulator can provide both components prior to the subtraction operation. Although the objective functions we analyzed did not depend on the ordering of the N simulated signal values, the view ordering must be supplied to functions that optimize some temporal or spectral characteristic of the signal profile. Also, other k-space trajectories besides spin-warp can be considered by altering the time at which the simulator calculates the average magnetization in each TR interval. Finally, by modifying the computational model to simulate a nonsubtractive free induction acquisition, this method will be applicable to standard, nonsubtractive steady-state free precession applications.

CONCLUSIONS

The proposed approach uses Bloch simulation and an efficient multistage optimization algorithm to find the transient bSSFP VFA schedule that optimizes an objective

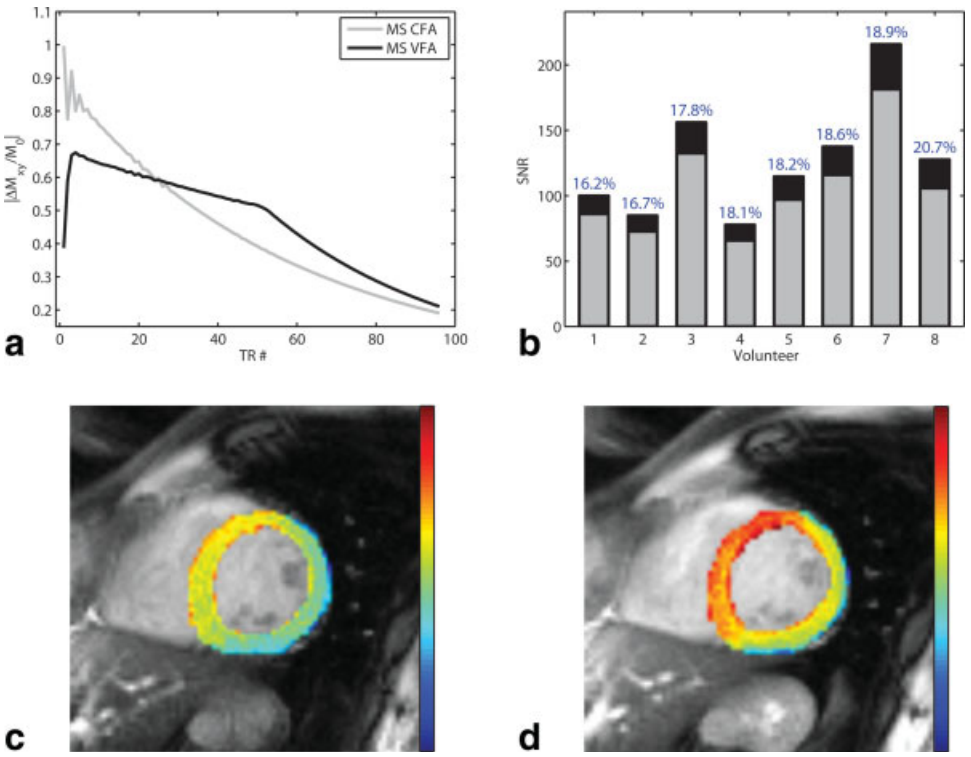

FIG. 3. Myocardial tissue results for the maximum sum (MS) objective function in Eq. 1, demonstrating the increased SNR obtained using the VFA schedule. **a**: Simulated signals showing a larger gain near the center of k-space with the VFA schedule. **b**: SNR measurements for the eight volunteers using the CFA (gray) and VFA (black) schedules. The SNR improvement, defined as $(SNR_{VFA}/SNR_{CFA}-1) \times 100$, is displayed above each bar. Example short-axis difference images from volunteer #4 acquired with (**c**) the CFA schedule and (**d**) the VFA schedule from volunteer #4 exhibiting the increase in myocardial signal and lack of image artifacts.

metric of the detected signal acquired from a differentially prepared magnetization scheme. Three flip angle schedules were generated under different objective functions to demonstrate the versatility of this method and the accuracy of the simulation. In two different phantoms, the measured signals matched prediction very well, with a 0.92% mean normalized absolute error. A variable angle schedule to increase the SNR in myocardial tissue was generated. In eight healthy volunteers, this schedule produced an 18.2% mean SNR improvement over the conventional CFA approach without introducing artifacts in the difference images.

APPENDIX

In each stage, the N-angle schedule is represented by an F-segment piecewise constant function. When N/F is a positive integer, the schedule consists of F segments, with each segment containing a flip angle repeated N/F times. When N/F is rational but not a positive integer, the segments can no longer be of equal size. Defining $P = N - \lfloor N/F \rfloor \cdot F$, the schedule has P segments, each with $\lceil N/F \rceil$ angles, and $F - P$ segments each with $\lfloor N/F \rfloor$ angles. The $F - P$ segments are uniformly interspersed among the P larger segments. For example, if $N = 16$ and $F = 7$, then the piecewise representation is $\{\alpha_1\ \alpha_1\ \alpha_2\ \alpha_2\ \alpha_3\ \alpha_3\ \alpha_4\ \alpha_4\ \alpha_4\ \alpha_5\ \alpha_5\ \alpha_6\ \alpha_6\ \alpha_7\ \alpha_7\ \alpha_7\}$, where α_i is the angle for the ith segment.

REFERENCES

1. Calamante F, Thomas DL, Pell GS, Wiersma J, Turner R. Measuring cerebral blood flow using magnetic resonance imaging techniques. J Cereb Blood Flow Metab 1999;19:701–735.
2. Koktzoglou I, Edelman R. STAR and STARFIRE for flow-dependent and flow-independent noncontrast carotid angiography. Magn Reson Med 2009;61:117–124.
3. Priest AN, Graves MJ, Wong P, Lomas DJ. Flow-dependent arterial and venous imaging by non-contrast-enhanced subtraction angiography. In: Proceedings of the 16th Annual Meeting of ISMRM, Toronto, 2008. p 727.
4. Aletras AH, Ding S, Balaban RS, Wen H. DENSE: displacement encoding with stimulated echoes in cardiac functional MRI. J Magn Reson 1999;137:247–252.
5. Huang TY, Liu YJ, Stemmer A, Poncelet BP. T2 measurement of the human myocardium using a T2-prepared transient-state trueFISP sequence. Magn Reson Med 2007;57:960–966.
6. An J, Voorhees A, Chen Q. SSFP arterial spin labeling myocardial perfusion imaging at 3 tesla. In: Proceedings of the 15th Annual Meeting of ISMRM, Miami, 2005. p 253.
7. Scheffler KS. Principles and applications of balanced SSFP techniques. Eur Radiol 2003;13:2409–2418.
8. Martirosian P, Klose U, Mader I, Schick F. FAIR true-FISP perfusion imaging of the kidneys. Magn Reson Med 2004;51:353–361.
9. Zun Z, Wong EC, Nayak KS. Assessment of myocardial blood flow in humans using arterial spin labeling: feasibility and SNR requirements. Magn Reson Med. 2009;62:975–983.
10. Nayak KS, Lee HL, Hargreaves BA, Hu BS. Wideband SSFP: alternating repetition time balanced steady state free precession with increased band spacing. Magn Reson Med 2007;58:931–938.
11. Hargreaves BA, Vasanawala SS, Pauly JM, Nishimura DG. Characterization and reduction of the transient response in steady-state MR imaging. Magn Reson Med 2001;46:149–158.
12. Le Roux P. Simplified model and stabilization of SSFP sequences. J Magn Reson 2003;163:23–37.
13. Fletcher R. Practical methods of optimization. New York: John Wiley & Sons; 1987. 450 p.
14. Gill PE, Murray W, Wright MH. Numerical linear algebra and optimization, vol. 1. Redwood City, CA: Addison Wesley; 1991. 448 p.
15. Staewen RS, Johnson AJ, Ross BD, Parrish T, Merkle H, Garwood M. 3-D FLASH imaging using a single surface coil and a new adiabatic pulse, BIR-4. Invest Radiol 1990;25:559–567.
16. Insko EK, Bolinger L. B1 mapping. In: Proceedings of the 111th Annual Meeting of ISMRM, Berlin, 1992. p 106.
17. Noeske R, Seifert F, Rhein KH, Rinneberg H. Human cardiac imaging at 3T using phased array coils. Magn Reson Med 2000;44:978–982.
18. Sung K, Nayak KS. The design and use of tailored hard-pulse trains for uniform saturation of myocardium at 3 tesla. Magn Reson Med 2008;60:997–1002.